Evaluating Uncertainty and Modes of Variability for Antarctic Atmospheric Rivers

Christine A Shields[1], Jonathan D Wille[2], Allison B. Marquardt Collow[3], Michelle Laura Maclennan[4], and Irina Gorodetskaya[5]

[1]National Center for Atmospheric Research (UCAR)
[2]Université Grenoble Alpes
[3]Universities Space Research Association and NASA/GSFC
[4]University of Colorado Boulder
[5]University of Aveiro

November 22, 2022

Abstract

Antarctic atmospheric rivers (ARs) are driven by their synoptic environments and lead to profound and varying impacts along the coastlines and over the continent. The definition and detection of ARs specifically over Antarctica accounts for large uncertainty in AR metrics, and consequently, impacts quantification. We find that Antarctic-specific detection tools consistently capture the AR footprint inland over the ice sheets, whereas most global detection tools do not. Large-scale synoptic environments and associated ARs, however, are broadly consistent across detection tools. Using data from the Atmospheric River Tracking Method Intercomparison Project and global reanalyses, we quantify the uncertainty in Antarctic AR metrics as well as evaluate large-scale environments in the context of decadal and interannual modes of variability. The Antarctic western hemisphere has stronger connections to both decadal and interannual modes of variability compared to East Antarctica, and the IOD's influence on Antarctic ARs is stronger while in phase with ENSO.

Evaluating Uncertainty and Modes of Variability for Antarctic Atmospheric Rivers

Christine A. Shields[1], Jonathan D. Wille[2], Allison B. Marquardt Collow[3,4], Michelle Maclennan[5], Irina V. Gorodetskaya[6]

[1]National Center for Atmospheric Research, Climate and Global Dynamics Laboratory, Boulder, Colorado

[2]Institut des Géosciences de l'Environnement, CNRS/UGA/IRD/G-INP, Saint Martin d'Hères, France

[3]University of Maryland Baltimore County, Baltimore, MD

[4]Global Modeling and Assimilation Office, NASA Goddard Space Flight Center, Greenbelt, MD

[5]University of Colorado, Department of Atmospheric and Oceanic Science, Boulder, Colorado

[6]CESAM – Centre for Environmental and Marine Studies, Department of Physics, University of Aveiro, Aveiro, Portugal

Corresponding author: Christine A. Shields (shields@ucar.edu)

Key Points:

- Antarctic-specific AR detection tools better capture continental interior footprint
- Modes of variability (MOVs) generally hold greater influence over West Antarctica than East Antarctica and are consistent across most ARDTs
- IOD teleconnections in phase with ENSO produce a stronger AR precipitation response compared to other MOVs

Abstract

Antarctic atmospheric rivers (ARs) are driven by their synoptic environments and lead to profound and varying impacts along the coastlines and over the continent. The definition and detection of ARs specifically over Antarctica accounts for large uncertainty in AR metrics, and consequently, impacts quantification. We find that Antarctic-specific detection tools consistently capture the AR footprint inland over the ice sheets, whereas most global detection tools do not. Large-scale synoptic environments and associated ARs, however, are broadly consistent across detection tools. Using data from the Atmospheric River Tracking Method Intercomparison Project and global reanalyses, we quantify the uncertainty in Antarctic AR metrics as well as evaluate large-scale environments in the context of decadal and interannual modes of variability. The Antarctic western hemisphere has stronger connections to both decadal and interannual modes of variability compared to East Antarctica, and the IOD's influence on Antarctic ARs is stronger while in phase with ENSO.

Plain Language Summary

Atmospheric rivers (ARs) are large-scale weather features that transport significant amounts of moisture and are akin to “rivers in the sky”. ARs traveling to Antarctica from the mid-latitudes can bring enough moisture to produce extreme snowfall, or if accompanied by warm air, can result in melt events, both of which affect ice sheets across the continent. How we define ARs in gridded datasets significantly impact what we say about them. If a definition uses Antarctic-specific constraints, it does a better job at describing the actual spatial footprint with increasing importance the further inland the impact. The large-scale environments that produce ARs, and how these environments naturally vary, however, are generally consistent regardless of how we define ARs. ARs impacting the western hemisphere of Antarctica are more deeply connected to specific atmospheric patterns that repeatedly occur compared to weaker connections with East Antarctic ARs.

1 Introduction

Atmospheric rivers (ARs) are long, narrow synoptic-scale weather phenomena that serve as meridional transport vehicles important for both large-scale and local hydrological climate across the globe. ARs transport both water and energy from lower to high latitudes and are often connected to extratropical cyclones where moisture laden bands of water vapor and clouds extend and travel across and along baroclinic zones (Ralph et al., 2018, AMS Glossary of Meteorology, 2017). Although the bulk of the current literature describe ARs in mid-latitude locations impacting western coasts of continents, such as western North America and western Europe, ARs are equally important in polar regions where the interaction of these moisture streams with land and sea ice, result in consequential precipitation events impacting the local cryosphere (Turner et al., 2019, Mattingly et al., 2018). Specific to Antarctica and depending on the thermal characteristics, ARs can produce significant snow accumulation over the ice sheet, (Gorodetskaya et al. 2014, Adusumilli et al. 2021, Terpstra et al. 2021, Wille et al., 2021), or melt events with consequences for ice shelf stability (Wille et al. 2019, Wille et al., 2022, Turner et al. 2022, Clem et al., 2022). Generally, ARs reaching Antarctica are relatively rare occurrences (Wille et al., 2021), fully extending into the continent only a few times per year but clearly tied to favorable synoptic conditions, such as dominate blocking events in the Southern Ocean that funnel ARs into the continent (Wille et al. 2021, Pohl et al., 2021, Maclennan et al. 2021, Bozkurt et al. 2018, Terpstra et al. 2021). Teleconnections and modes of natural variability (MOVs) can be tied to synoptic conditions favorable for AR occurrences around different regions of Antarctica, such as the Southern Annular Mode (SAM) (Wille et al., 2021, Clem et al. 2016, Raphael et al., 2016, Marshall et al. 2016), the Pacific South American Mode 2 (PSA2) (Maclennan et al., 2021, Marshall et al. 2016), the Pacific Decadal Oscillation (PDO) (Turner et al. 2019, Fogt et al. 2019), the Indian Ocean Dipole and El Nino Southern Oscillation (IOD, ENSO, respectively) (Nuncio and Yuan, 2015). Parts of the cold temperature anomalies in West Antarctica can also be explained by the influence of the Indian Ocean Basin mode and Atlantic Zonal and Meridional Modes (Li et al., 2015; Lee and Jin, 2021; Gutierrez et al., 2021, Table Atlas.1). In this study, we explicitly evaluate the relationship between these MOVs, ARs, and their associated precipitation and boundary layer temperature, to characterize the varied impacts across different regions and flavors of ARs. Although we do not consider here an exhaustive list of MOVs of consequence for ARs, we limit this study to the decadal and interannual bimodal indices of variability introduced here. Additionally, because the very definition an AR is often debated (i.e., is the feature simply a moisture transport alone, or rather, connected to an extratropical cyclone) (Shields et al., 2019, Ralph et al., 2018, Gimeno et al., 2021) we quantify the uncertainties in AR metrics such as occurrence and climatology, as well as MOV impact, to provide context for our results.

2 Data and Methods

2.1 Reanalysis Datasets

We employ both the Modern Era Retrospective Analysis for Research and Applications, version 2 (MERRA-2) (Gelaro et al., 2017) and European Centre for Medium-Range Weather Forecasts' Reanalysis Version 5 (ERA5) (Hersbach et al., 2020) global reanalyses in this work. To represent large scale synoptics and analyze modes of variability, we primarily use MERRA-2, which explicitly represents the energy and hydrologic budgets over ice sheets in Antarctica (Gelaro et al., 2017). A more in-depth evaluation of the cryosphere in MERRA-2 is available in

Section 9 of Bosilovich et al. (2015) as well as Gossart et al. (2019). Sea surface temperature and sea ice concentration in MERRA-2 are prescribed as indicated by Table 3 of Gelaro et al. (2017). At approximately 50 km resolution, MERRA-2 is sufficient to resolve weather features, such as atmospheric rivers, along with their associated precipitation, and is the baseline dataset for the Atmospheric River Tracking Method Intercomparison Project (ARTMIP) (Shields et al., 2018, Rutz et al., 2019). ARTMIP provides a collection of AR "catalogues" from a variety of ARDTs (Atmospheric River Detection Tools) that detail gridded and timeslice information on where and when ARs exist. Using MERRA-2 across the same years as included in ARTMIP (1980-2016) allows us to consistently apply all available ARTMIP ARDT catalogues to Antarctic AR uncertainty quantification. ERA5 datasets are also applied (1980-2020), where available, to further represent the spread in climatology metrics across both ARDT and reanalysis products. Monthly MERRA-2 data is used to compute MOV indices (GMAO, 2015a; GMAO, 2015b), daily data to compute precipitation (GMAO, 2015c) and 850 hPa temperature (GMAO, 2015d) for AR days, and 3-hourly data is used for AR identification (GMAO, 2015d). Only ARDTs with polar constraints (here referred to as P-ARTMIP) are used for MOV analysis to minimize errors by only including appropriately designed ARDTs.

2.2. Atmospheric River Detection

Identification and tracking of ARs require decisions dependent on the AR definition. Because this definition varies wildly from one project to another (Ralph et al. 2018, Rutz et al., 2019), metrics such as AR frequency and seasonality differ depending on choice of ARDT. ARTMIP has shown that uncertainty based on ARDT far outweighs uncertainty based on model (O'Brien et al., 2021) as well as reanalysis (Collow et al., 2022). Thus, uncertainty quantification is an important component to any analysis where AR detection is required. It is also important to recognize that applying many different ARDTs for each science problem is not always practical for individual researchers, so a balance must be struck where uncertainty due to ARDT is addressed by either explicit quantification or put into context relative to other ARDTs and determine if the chosen ARDT is fit for purpose (Rutz et al. 2019). Traditional ARDTs designed for the mid-latitudes typically apply moisture thresholds using the quantity called integrated vapor transport (IVT). However, for ARs making landfall and extending poleward onto the continent, one option is to identify ARs by simply using the meridional component. Here, we primarily apply Antarctic-specific ARDTs to diagnose the relationship between MOVs and ARs across Antarctica but include all methods with polar constraints to represent uncertainty spread. For climatology metrics, we include all available global ARTMIP ARDTs to highlight the large differences in metrics. The Antarctic-specific algorithms, herein referred to as Wille_vIVT and Wille_IWV, focus on meridional geometry and filter for high (98% percentile) relative moisture flow into the continent to better capture ARs impacting polar latitudes, rather than zonally around the Southern Ocean. Further details on Wille the ARDTs (Wille et al. 2019, Wille et al., 2021), ARTMIP ARDTs, and IVT/IWV calculations are in Supplemental.

2.3 Modes of Variability

We calculate both decadal and interannual modes of variability consistent with the Climate Variability and Diagnostic Package (CVDP) developed by Phillips et al., 2014. Modes were chosen based on current literature, as described in the introduction, regarding AR impacts in and around Antarctica. Decadal modes are represented here by the SAM and the PDO, and for interannual modes, PSA2 and IOD, both in and out of phase with ENSO. Specific details on computation are found in supplemental material. One caveat to using the PDO is the relatively short timespan of available data of ~four decades. Tropical pacific decadal variability (TPDV) such as the PDO have timescales from 8 to 40 years (Power et al., 2021), making significance testing challenging. Because we are limited to the ARTMIP time period and thus only 37 years are used, PDO and AR correlations are shown for qualitative illustration, but significance inferences are limited and used with caution.

3 Climatological characteristics and uncertainty due to ARDT

ARs impacting high latitude locales such as Antarctica do not necessarily follow mid-latitude storm tracks. Rather, ARs often bend and flow around high-pressure blocks or follow baroclinic zones connected to low pressure regimes ultimately pushing moisture intrusions into the continent. ARs that make it onto the continent are dominated by the north-south meridional component of the wind. This can be demonstrated by computing heat maps of AR occurrence for each method and comparing the Antarctic specific occurrences to traditional methods developed for mid-latitudes. Figure 1a shows the spatial distribution differences between the mean Wille Antarctic-specific ARDTs and the ARTMIP mean. ARs that make landfall are generally rare (a few times per year, Wille et al., 2021), but even so, the Antarctic specific ARDTs consistently detect ARs in the interior of the continent where most traditional ARDTs detect more in the Southern Ocean. Even global ARDTs that allow for polar thresholds (P-ARTMIP) (Figure 1b) ultimately do not capture ARs on the interior ice sheets, especially over East Antarctica. This is likely because the Antarctic specific ARDTs applied here focus on the meridional component of the moisture transport that allows for AR detection deeper into the dry Antarctic interior.

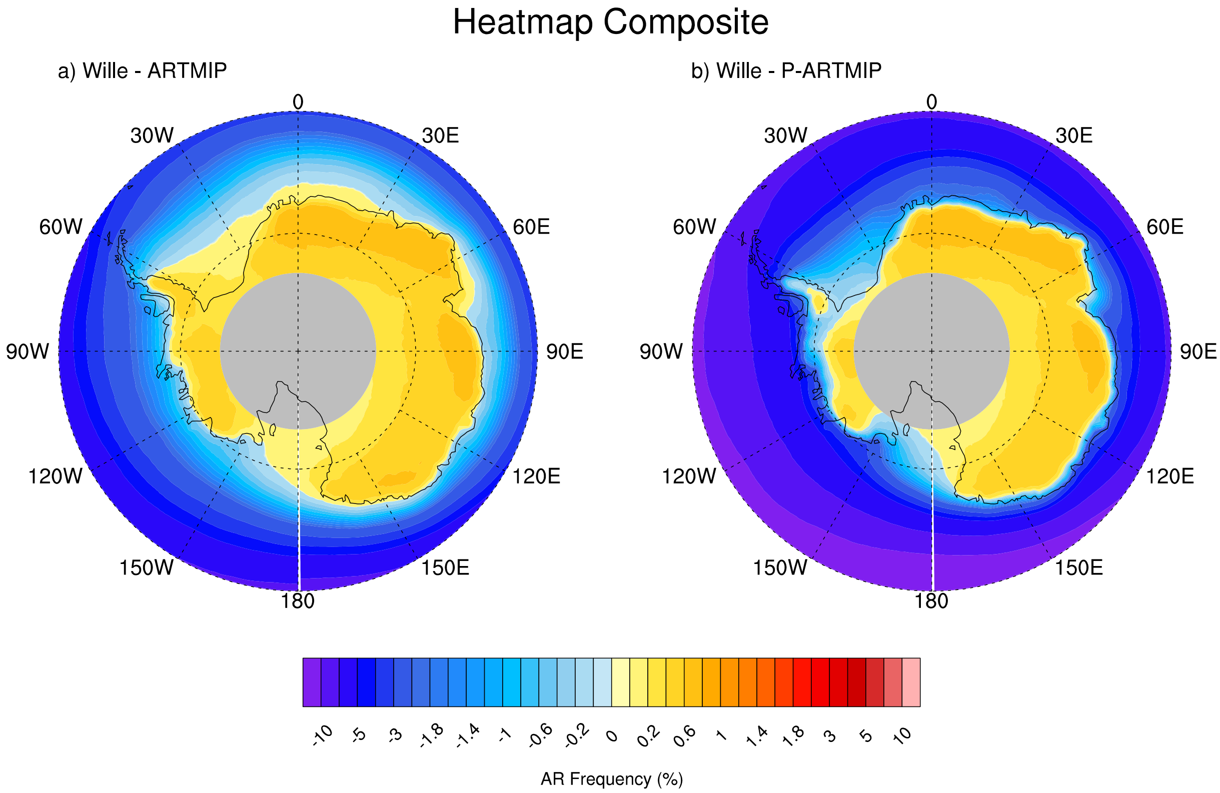

Figure 1. Composite difference heatmaps of AR frequency in % time (relative to MERRA-2 years 1980-2016). Wille ARDTs versus all applicable global ARDTs (a) and Wille ARDTs versus P-ARTMIP ARDTs that incorporate lower threshold constraints designed for polar latitudes (b).

From a continent-wide, climatological perspective, (Figure 2), the Wille ARDTs detect ARs distributed throughout the year, with maximum occurrence in Austral fall and winter, consistent with instrumental observations and a regional climate model that show high accumulation events with synoptic conditions for both West Antarctica over Thwaites Glacier (Maclennan et al., 2021, Lenaerts, et al., 2018) and East Antarctica over Dronning Maud Land (Gorodetskaya et al. 2014). Distinctly different from Wille ARDTs, ARs detected from global and P-ARTMIP methods, peak in February and Austral Fall, and are likely due to the dominance of the Antarctic Peninsula, which in some cases, are the only location where ARs are identified (Supplemental Figures 3 and 4). Because of the geographic position of the Peninsula in the Southern Ocean, the global ARDTs, designed for mid-latitudes, capture more zonally-oriented ARs. Specific regional climatologies (Antarctic Peninsula, Dronning Maud Land, and Princess Elizabeth/Queen Mary Lands) can be found in Supplemental.

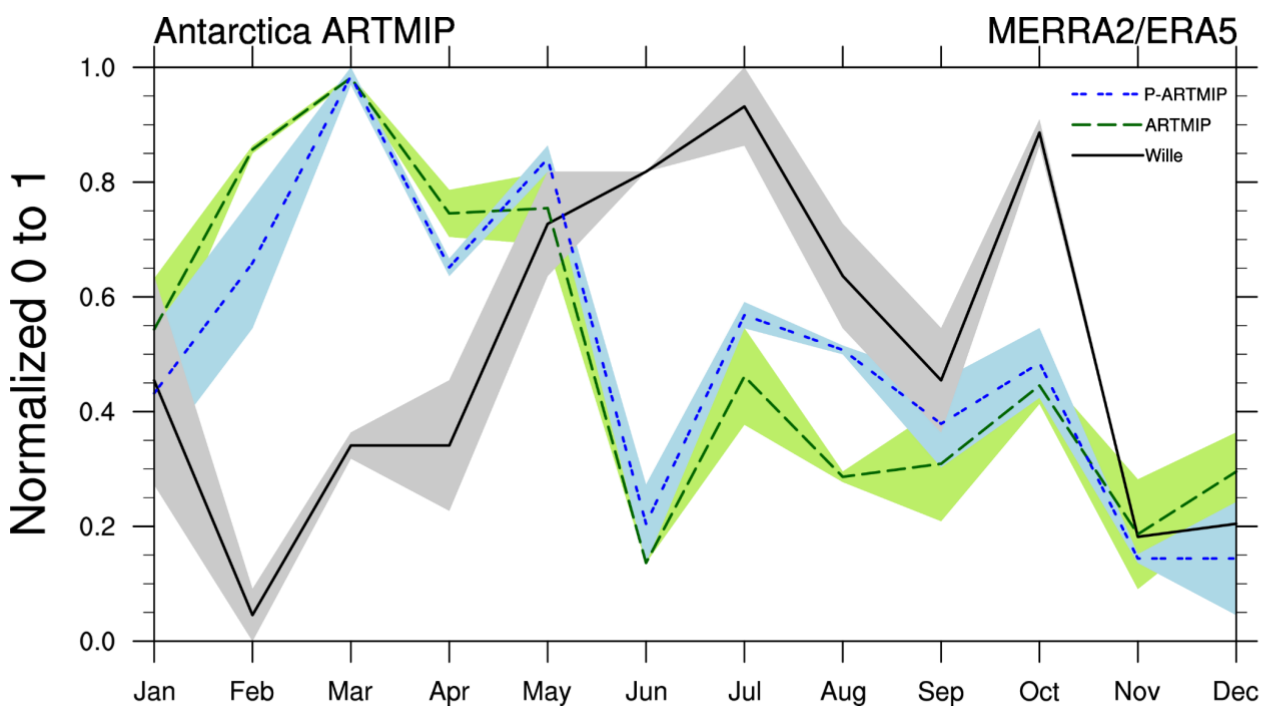

Figure 2. Antarctic seasonal cycle of ARs for ARTMIP mean (lines) and spread (shading) which includes applicable available ARDTs (Supplemental S1) and both reanalysis datasets ARTMIP Tier 1 MERRA-2 and Tier 2 ERA5. All available global ARDTS (ARTMIP) versus ARMIP with polar constraints (P-ARTMIP) versus Antarctic specific (Wille ARDTs).

4 Relationship between Antarctic ARs and MOVs

4. 1 MOV Synoptics for AR days

Around and across Antarctica, there are a variety of different climate regimes, but coastal climates depend on geometry and orientation of the coast relative to the zonal and meridional flow. However, for the purposes of evaluating broad synoptic influences, we divide our study into West and East Antarctica. To isolate and amplify unique west and east hemispheric patterns, we apply the split hemisphere technique, commonly used for peak (seasonal) tropical cyclone track density analysis (Korty et al., 2012, Yan et al., 2016), except here, we composite synoptic conditions for landfalling ARs for each, respective hemisphere. That is, for days where ARs impact West Antarctica, synoptic conditions are composited for the western hemisphere, and for days where ARs impact East Antarctica, synoptic conditions are composited for the eastern hemisphere. All spatial figures presented here contain a solid thick line dividing as a reminder that the hemispheres are treated separately but plotted together for illustration. We highlight the Wille_vIVT ARDT because this algorithm better represents AR dynamics (Wille et al., 2021). Figure 3 plots annual anomalies for low-level (850 hPa) moisture flux (vectors) and temperature (contours) for AR days occurring during the different phases of SAM and PSA, a decadal and interannual mode of variability, respectively, that represents variations in the dynamics. Across polar ARDTS (Fig. 3 e-h), clearly show the fluxes in (SAM positive Antarctic Peninsula, PSA2 negative for the West Antarctic Ice Sheet, Amundsen and Ross Seas) and out of the continent for the western hemisphere, consistent with Antarctic MOV patterns in Marshall and Thompson (2016) and Marshall et al. (2017). For East Antarctica, the fluxes are varied but generally the opposite, with, for example, Dronning Maud Land showing fluxes into the continent during SAM negative. Overall PSA2 holds greater influence for the western hemisphere, and results are consistent across all global ARDTs, regardless of polar constraints or not (not shown). Across ARDTs for AR days, although there are variations in boundary layer temperature, moisture, and winds, synoptic conditions are robust across methods, unlike frequency metrics and seasonal climatology although some regional differences exist from Wille_vIVT (Fig 3 i-l), our primary method. For example, SAM-, the Wille_vIVT ARDT detects more ARs with onshore flow to Terre Adelie Land (Fig 3l).

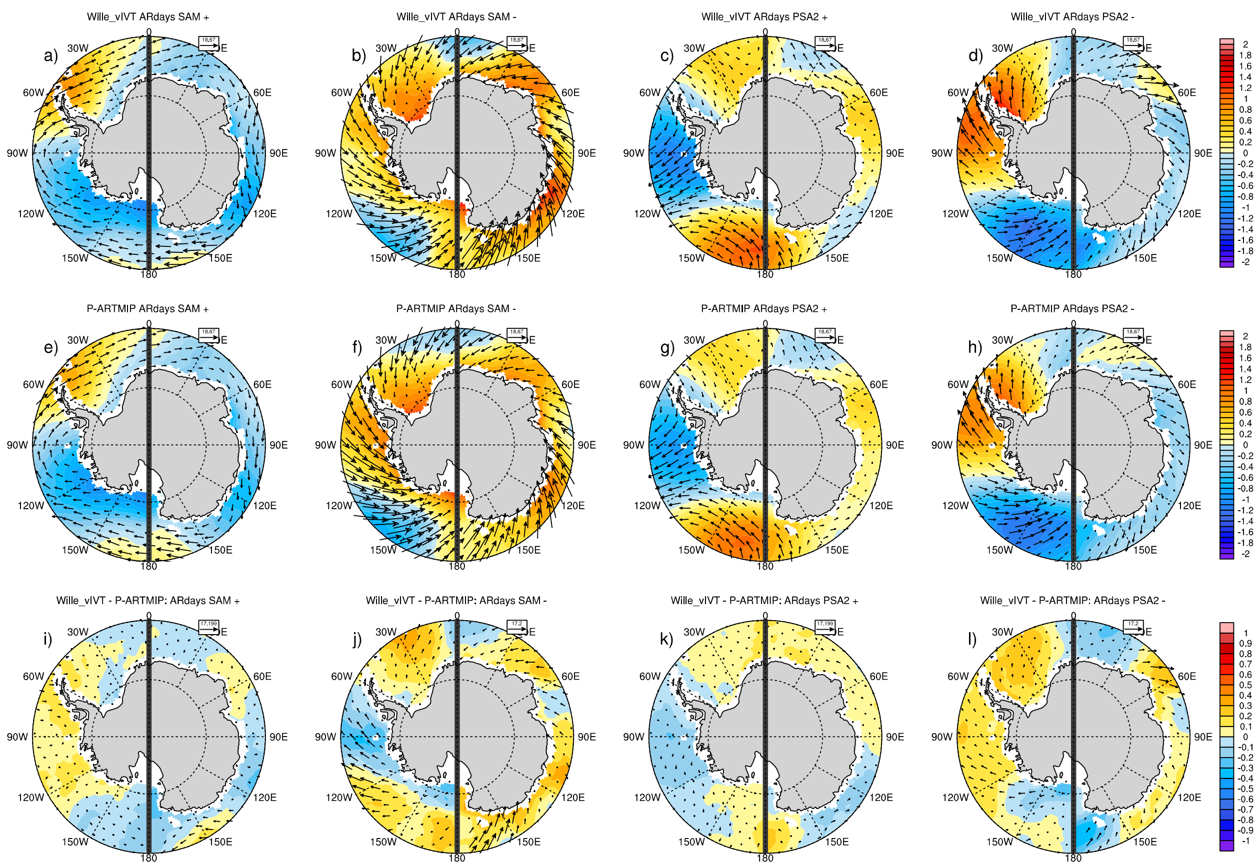

Figure 3. Anomalies of 850 hPa Air temperature for AR day composites (color contours) and 850 hPa moisture flux ($kgm^{-1}s^{-1}$)(arrows) during SAM phases (a-b,e-f,i-j), PSA2 phases (c-d,g-h,k-l) in split hemisphere format. West Antarctic ARs are composited separately from East Antarctic ARs to maintain unique hemispheric synoptic signatures and combined for illustration, separated by thick gray line. Wille_vIVT (a-d), ARTMIP mean for ARDTs with polar constraints (P-ARTMIP) (e-h) and differences (i-l) are shown.

4.2 Precipitation and temperature impacts

4.2.1 Decadal modes of variability: SAM and PDO

Decadal modes of variability, their relationship with AR precipitation and 850 hPa temperature, and ARTMIP uncertainty, is shown in Figure 4. Again, we highlight the Wille_vIVT ARDT for spatial plots that regress PC timeseries for SAM (Fig. 4b, e) and PDO (Fig. 4c, f) onto precipitation and temperature anomalies for AR days. For the PDO, we show western hemisphere only due to the lack of any significance elsewhere. Both precipitation and temperature follow the composite plots for AR days (Fig. 3) in that where moisture fluxes flow into the continent, enhanced precipitation occurs, along with corresponding temperature anomalies. For example, SAM in the positive phase typically indicates a deeper Amundsen Sea Low (and vice-versa), and generally less mass transport between Antarctica and the southern mid-latitudes (Turner et al., 2013, Spensberger et al., 2020). Figure 4b shows the precipitation is positively and significantly correlated with SAM over Antarctic Peninsula (label A) and negatively correlated over the Amundsen sea region (label B), resulting from a deeper Amundsen Sea Low that brings cyclonic, clockwise flow into the Peninsula and out of the Amundsen sea region during SAM positive. SAM negative, oppositely correlated with precipitation between Amundsen and Ross Seas near Marie Byrd Land, supports onshore flow during the negative phase. The eastern hemisphere shows less significance in precipitation although SAM's influence is hinted at in regions such as Dronning Maud Land, Kemp Land and the Amery Ice Shelf, and Wilkes Land (labels C, D, E, respectively; supplemental Figure S1 for Antarctic locations). The PDO shows a negative correlation with the Antarctic Peninsula in both temperature and precipitation (labels K, F), and a positive one between the Amundsen and Ross Seas (labels L, G), although significance is weak and overall shows less influence than SAM. Each region that shows significance is tested across all P-ARTMIP algorithms (Fig. 4a, d) to quantify uncertainty in these calculations. Across most regions and methods, the sign of the correlation is robust for both temperature and precipitation, except for Dronning Maud Land (DML) for precipitation (label C), where the strength of the correlation is generally tied to frequency climatology.

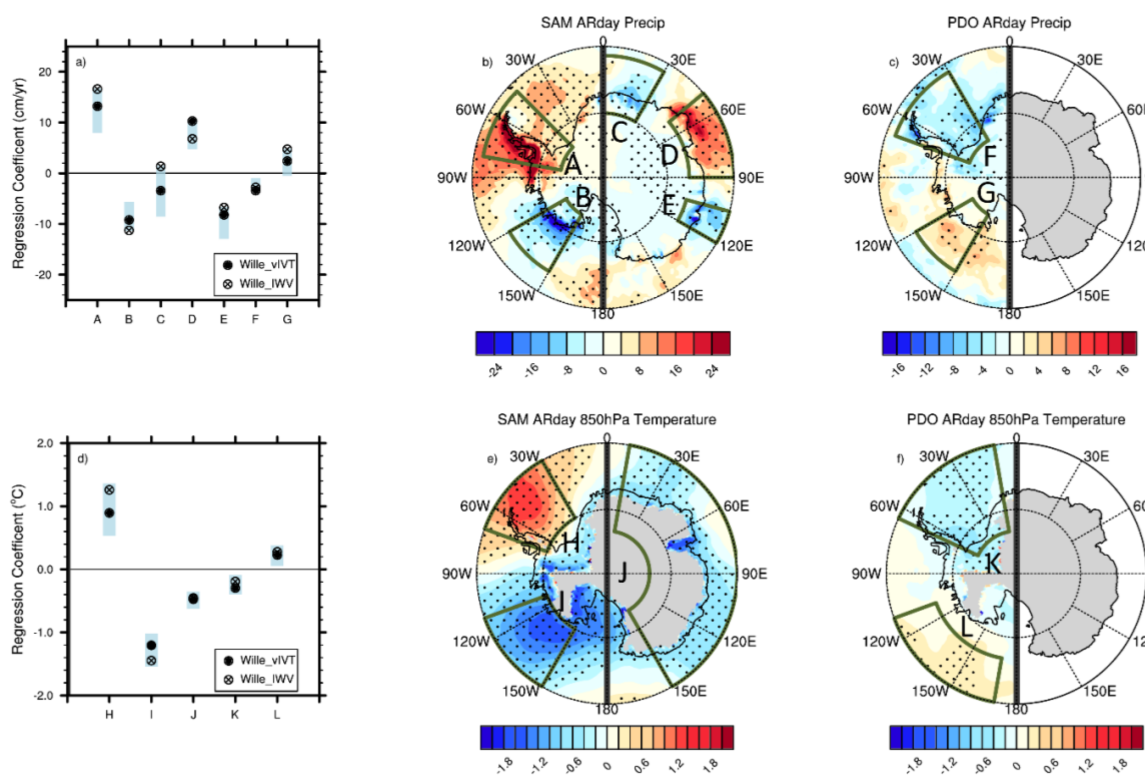

Figure 4. Regression patterns and spread for AR days and decadal modes of variability (SAM and PDO). Precipitation ($cmyr^{-1}$) (b-c) and 850 hPa temperature (ºC) (e-f) patterns are plotted for Wille_vIVT ARDT. Uncertainty is shown for area-averaged regression values across all P-ARTMIP ARDTs (a,d). Dark green boxes indicate areas used in the uncertainty calculation and are labeled alphabetically. Split hemisphere format, as Figure 3, is used. The PDO is shown for western hemisphere only. Significance was tested at 90% level using a student T-test. Where shown, 850 hPa temperatures are plotted for topographical regions under 850 hPa highlighting coastal and escarpment zones and eliminating errors on pressure surfaces due to elevation.

4.2.2 Interannual modes of variability: PSA2, IOD and ENSO

Interannual modes of variability, their relationship with AR precipitation and 850 hPa temperature, and ARTMIP uncertainty, is shown in Figure 5. We evaluate PSA2 and IOD independently to illustrate their dominant, spatial impacts. However, it is important to note that no MOV, and especially interannual modes, operate in isolation. The PSA2 mode has been shown to excite sea surface temperature (SST) patterns tied to the evolution of ENSO (Lou et al., 2021), and the IOD is often paired with ENSO, in addition to decadal modes such as PDO. For simplicity, we evaluate the dynamical mode of PSA2 separately from modes defined by SST anomalies (IOD, ENSO). The PSA2 has already been shown to have significant implications for the Amundsen Sea Embayment and Thwaites Glacier (Maclennen et al. 2021), and we confirm this with our regression analysis that shows negative correlation with PSA2 and precipitation in this area (label B), consistent with flux composites in Figure 3 and a potential amplification of wavenumber 3 (Cai et al., 1999). Temperature anomalies for AR days also align with regressions where poleward flow from mid-latitudes brings warmth into the Ross Sea region and is positively correlated with PSA2 (label N) compared to equatorward flow, negative correlations, and colder temperature over Amundsen Sea (label M). The IOD (Fig 5c-d, g-h) is much more potent while in phase with ENSO with negative correlations over West Antarctic regions such as Ellsworth Land (labels GG, PP) and positive correlations with Eastern Dronning Maud Land (label II) and Ross Sea (labels HH, QQ). Temperature significance is stronger than precipitation significance, however, likely tied to the broad extratropical SST influences during these modes. Although significance with Wille_vIVT is strong for temperatures, the differences with Wille_IWV and the P-ARTMIP spread (Fig5 a, e) suggest this result is not necessarily robust across ARDTs, and even potentially changes the sign of the correlation. Precipitation uncertainty is smaller, with most of the methods agreeing on correlation signs except for the IOD responses near Wilkes Land (label KK). Finally, the amplitude of IOD-ENSO response is much higher than any other MOV, interannual or decadal, suggesting that the IOD in phase with ENSO produces more anomalous precipitation than any other mode studied here. Nuncio and Yuan (2015) describe Antarctic sea ice correlations during IOD with ENSO in the Pacific sector and Ross Seas, and note the decrease is sea ice corresponding to warm meridional flow. Additionally, the wave train schematic in Nuncio and Yuan (2015) is consistent with our results that show for AR days, precipitation and warm low-level temperatures are positively correlated due to enhanced poleward flow at the Ross Sea and equatorward flow off the West Antarctic Ice Sheet.

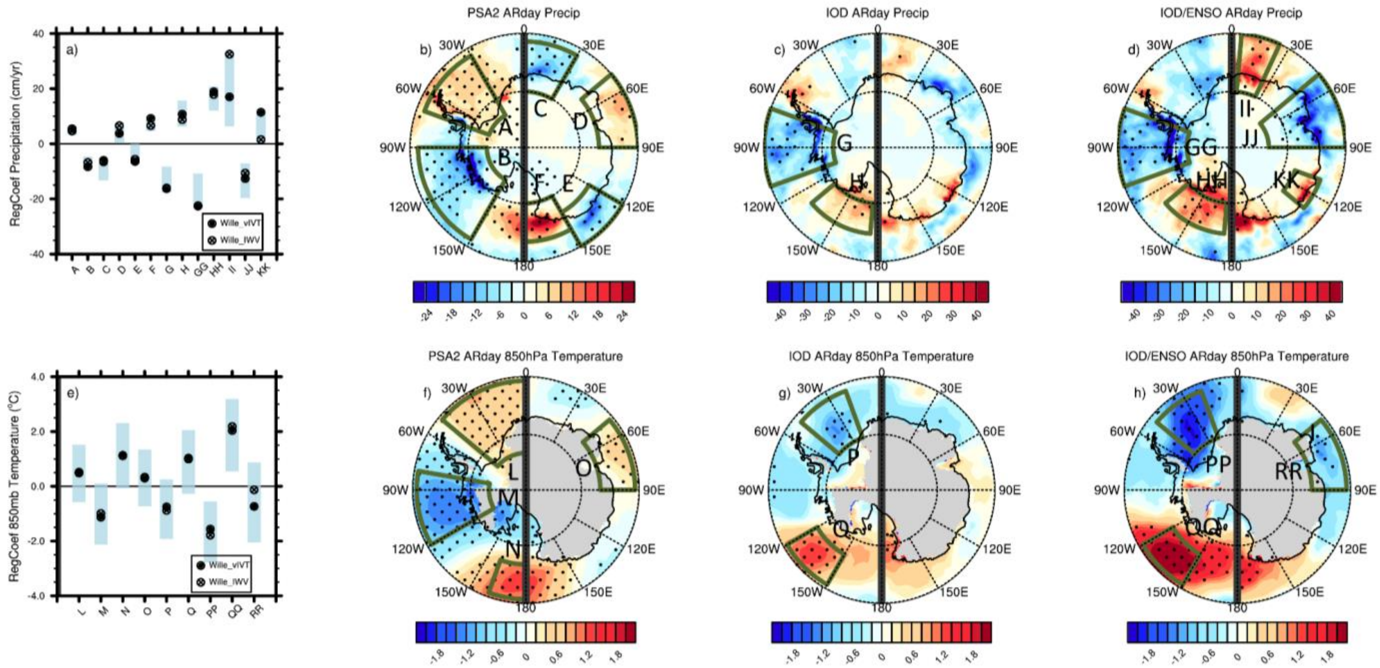

Figure 5. Same as Fig 4 except for interannual modes of variability PSA2 (b,f), IOD without (c,g) and IOD in phase with ENSO (d,h). Significance was tested at 90% level using a student T-test. Note precipitation contour scales are different for PSA2 versus IOD.

5 Conclusions

Studying Antarctic atmospheric rivers combine a unique set of disciplines incorporating both atmospheric science and the cryosphere, but also cross-disciple interests such as feature detection. To understand this phenomenon, we must both define it and put it into context with current research. Antarctic AR detection tools are generally robust across the synoptic meteorology, however large uncertainties exist for AR frequency climatology metrics such as seasonal cycle and location of landfall. Antarctic-specific tools that rely on the meridional characteristics of ARs capture the continental interior footprint of ARs more consistently compared to global ARDTs designed for the mid-latitudes. When evaluating ARs in the context of modes of natural variability (SAM, PSA2, PDO, IOD and ENSO), this study finds the MOVs studied here influence West Antarctic ARs more than East Antarctica. Spread among ARDTs is generally smaller for decadal modes of variability compared to interannual modes. This is likely due to the shorter period for interannual modes and the opportunity for compounding MOV events. Additionally, the Indian-ocean dipole teleconnections with ENSO produce a stronger AR response, mostly for West Antarctica and the Pacific sector, compared to other MOVs. Although we have chosen to diagnose MOVs that sample both decadal and interannual variability, it is not a complete list of potential influences on ARs onto the Antarctic glaciers and ice shelves. Future work includes understanding compound MOVs beyond IOD and ENSO. With our exploration of IOD and ENSO, compound MOVs clearly have the potential to amplify or suppress AR activity. Understanding the interplay between MOVs and ARs improves predictability and the ability to manage consequences as we move into a warmer climate. A future increase in MOVs that favor AR landfalls and warmer conditions will likely increase snowfall in the impacted area, but also risk increased surface melt and ice shelf destabilization.

Acknowledgments

This work is supported by the U.S. Department of Energy, Office of Science, Office of Biological & Environmental Research (BER), Regional and Global Model Analysis (RGMA) component of the Earth and Environmental System Modeling Program under Award Number DE-SC0022070 and National Science Foundation (NSF) IA 1947282 and by the National Center for Atmospheric Research (NCAR), sponsored by the NSF Cooperative Agreement No. 1852977. ARTMIP is a grass-roots community effort. Details on ARDTs can be found on the ARTMIP website, https://www.cgd.ucar.edu/projects/artmip/algorithms.html, but we specifically thank B. Guan, J. Lora, M. Krinisky, K. Kashinath, E.McClenny, K. Nardi, M. Pan, K. Reid, J. Rutz, T. O'Brien, E.Shearer, P. Ullrich, G. Xu) for their catalogues. ARTMIP DOE (BER) RGMA and the Center for Western Weather and Water Extremes (CW3E) at Scripps Institute for Oceanography at the University of California, San Diego. J. D. W. acknowledges support from the Agence Nationale de la Recherche project, ANR-20-CE01-0013 (ARCA). M. L. Maclennan acknowledges support from NASA FINESST grant 80NSSC21K1610.

Open Research

ARTMIP data is available from the Climate Data Gateway https://doi.org/10.5065/D6R78D1M and http://doi.org/10.5065/D62R3QFS. MERRA-2 is available from the Goddard Earth Sciences Data and Information Services Center (GES DISC) at https://disc.gsfc.nasa.gov/, DOI numbers doi: 10.5067/9SC1VNTWGWV3 and doi: 10.5067/Q5GVUVUIVGO7. ERA5 data is available from the Copernicus Climate Change Service (C3S) Climate Data Store at https://cds.climate.copernicus.eu/cdsapp#!/dataset/reanalysis-era5-single-levels?tab=overview.

References

Adusumilli, Susheel, Meredith A Fish, Helen Amanda Fricker, and Brooke Medley. (2021), Atmospheric river precipitation contributed to rapid increases in surface height of the west Antarctic ice sheet in 2019, *Geophysical Research Letters* 48, no. 5: e2020GL091076.

American Meteorological Society, (2017). Atmospheric river. Glossary of Meteorology, http://glossary.ametsoc.org/wiki/Atmospheric_river.

Bosilovich, M. G., and Coauthors, (2015). MERRA-2: Initial evaluation of the climate. *Technical Report Series on Global Modeling and Data Assimilation*, Vol. 43, NASA Tech. Rep. NASA/TM–2015–104606, 139 pp. [Available online at https://gmao.gsfc.nasa.gov/pubs/docs/Bosilovich803.pdf.]

Bozkurt, D., Rondanelli, R., Marin, J. C., & Garreaud, R. (2018). Foehn event triggered by an atmospheric river underlies record-setting temperature along continental Antarctica. *Journal of Geophysical Research: Atmospheres*, 123, 3871– 3892. https://doi-org.cuucar.idm.oclc.org/10.1002/2017JD027796

Cai, W., Baines, P. G., & Gordon, H. B. (1999). Southern Mid- to High-Latitude Variability, a Zonal Wavenumber-3 Pattern, and the Antarctic Circumpolar Wave in the CSIRO Coupled Model, *Journal of Climate*, 12(10), 3087-3104.

Clem, K. R., Renwick, J. A., McGregor, J., and Fogt, R. L. (2016), The relative influence of ENSO and SAM on Antarctic Peninsula climate, *J. Geophys. Res. Atmos*., 121, 9324– 9341, doi:10.1002/2016JD025305.

Clem, K.R., Bozkurt, D., Kennett, D., King, J., Turner, J. (2021). Central tropical Pacific convection drives extreme high temperatures and surface melt on the Larsen ice shelf, 11 August 2021, PREPRINT (Version 1) available at Research Square [https://doi.org/10.21203/rs.3.rs-712751/v1]

Collow, A. B. M., Shields, C. A., Guan, B., Kim, S., Lora, J. M., McClenny, E. E., et al. (2022). An overview of ARTMIP's Tier 2 Reanalysis Intercomparison: Uncertainty in the detection of atmospheric rivers and their associated precipitation. *Journal of Geophysical Research: Atmospheres*, 127, e2021JD036155, https://doi.org/10.1029/2021JD036155.

Francis, D., Mattingly, K. S., Temimi, M., Massom, R., & Heil, P. (2020). On the crucial role of atmospheric rivers in the two major Weddell Polynya events in 1973 and 2017 in Antarctica. *Science Advances*, 6(46), eabc2695.

Fogt, R.L. and Clem, K.R., (2020). Connections with middle and low latitudes. *In Past Antarctica* (pp. 219-239). Academic Press.

Gelaro, R., McCarty, W., Suárez, M. J., Todling, R., Molod, A., Takacs, L., Randles, C. A., Darmenov, A., Bosilovich, M. G., Reichle, R., Wargan, K., Coy, L., Cullather, R., Draper, C., Akella, S., Buchard, V., Conaty, A., da Silva, A. M., Gu, W., Kim, G., Koster, R., Lucchesi, R., Merkova, D., Nielsen, J. E., Partyka, G., Pawson, S., Putman, W., Rienecker, M., Schubert, S. D., Sienkiewicz, M., & Zhao, B. (2017). The Modern-Era Retrospective Analysis for Research and Applications, Version 2 (MERRA-2), *Journal of Climate*, 30(14), 5419-5454, https://doi.org/10.1175/JCLI-D-16-0758.1.

Gimeno, L., Algarra, I., Eiras-Barca, J., Ramos, A. M., & Nieto, R. (2021). Atmospheric river, a term encompassing different meteorological patterns. Wiley Interdisciplinary Reviews: Water, 8(6), e1558.

Global Modeling and Assimilation Office (GMAO) (2015a), MERRA-2 tavgM_2d_slv_Nx: 2d,Monthly mean,Time-Averaged,Single-Level,Assimilation,Single-Level Diagnostics V5.12.4, Greenbelt, MD, USA, Goddard Earth Sciences Data and Information Services Center (GES DISC), https://doi.org/10.5067/AP1B0BA5PD2K.

Global Modeling and Assimilation Office (GMAO) (2015b), MERRA-2 tavgM_2d_ocn_Nx: 2d,Monthly mean,Time-Averaged,Single-Level,Assimilation,Ocean Surface Diagnostics V5.12.4, Greenbelt, MD, USA, Goddard Earth Sciences Data and Information Services Center (GES DISC), https://doi.org/10.5067/4IASLIDL8EEC.

Global Modeling and Assimilation Office (GMAO) (2015c), MERRA-2 tavg1_2d_flx_Nx: 2d,1-Hourly,Time-Averaged,Single-Level,Assimilation,Surface Flux Diagnostics V5.12.4, Greenbelt, MD, USA, Goddard Earth Sciences Data and Information Services Center (GES DISC), https://doi.org/10.5067/7MCPBJ41Y0K6.

Global Modeling and Assimilation Office (GMAO) (2015d), MERRA-2 inst3_3d_asm_Np: 3d,3-Hourly,Instantaneous,Pressure-Level,Assimilation,Assimilated Meteorological Fields V5.12.4, Greenbelt, MD, USA, Goddard Earth Sciences Data and Information Services Center (GES DISC), https://doi.org/10.5067/QBZ6MG944HW0.

Gorodetskaya, I. V., Silva, T., Schmithüsen, H., & Hirasawa, N. (2020). Atmospheric river signatures in radiosonde profiles and reanal-yses at the Dronning Maud Land Coast, East

Antarctica. *Advances in Atmospheric Sciences*, 37(5), 455–476. https://doi.org/10.1007/s00376-020-9221-8

Gorodetskaya, I. V., Tsukernik, M., Claes, K., Ralph, M. F., Neff, W. D., & Van Lipzig, N. P. M. (2014). The role of atmospheric rivers in anomalous snow accumulation in East Antarctica. *Geophysical Research Letters*, 41(17), 6199–6206. https://doi.org/10.1002/2014GL060881

Gorodetskaya, I. V., Van Lipzig, N. P. M., Van den Broeke, M. R., Mangold, A., Boot, W., & Reijmer, C. H. (2013). Meteorological regimes and accumulation patterns at Utsteinen, Dronning Maud Land, East Antarctica: Analysis of two contrasting years. *Journal of Geophysical Research: Atmospheres*, 118(4), 1700–1715. https://doi.org/10.1002/jgrd.50177

Gossart, A., Helsen, S., Lenaerts, J. T. M., Broucke, S. V., van Lipzig, N. P. M., & Souverijns, N. (2019). An Evaluation of Surface Climatology in State-of-the-Art Reanalyses over the Antarctic Ice Sheet, *Journal of Climate*, *32*(20), 6899-6915, https://doi.org/10.1175/JCLI-D-19-0030.1.

Gutiérrez, J.M., R.G. Jones, G.T. Narisma, L.M. Alves, M. Amjad, I.V. Gorodetskaya, M. Grose, N.A.B. Klutse, S. Krakovska, J. Li, D. Martínez-Castro, L.O. Mearns, S.H. Mernild, T. Ngo-Duc, B. van den Hurk, and J.-H. Yoon, (2021). Atlas. In Climate Change 2021: The Physical Science Basis. Contribution of Working Group I to the Sixth Assessment Report of the Intergovernmental Panel on Climate Change [Masson-Delmotte, V., P. Zhai, A. Pirani, S.L. Connors, C. Péan, S. Berger, N. Caud, Y. Chen, L. Goldfarb, M.I. Gomis, M. Huang, K. Leitzell,

E. Lonnoy, J.B.R. Matthews, T.K. Maycock, T. Waterfield, O. Yelekçi, R. Yu, and B. Zhou (eds.)]. *Cambridge University Press*, Cambridge, United Kingdom and New York, NY, USA, pp. 1927–2058, doi:10.1017/9781009157896.021.

Hersbach, H., Bell, B., Berrisford, P., Hirahara, S., Horányi, A., Muñoz-Sabater, J., et al. (2020). The ERA5 global reanalysis. *Quarterly Journal of the Royal Meteorological Society*, 146, 1999–2049, https://doi.org/10.1002/qj.3803.

Korty, R. L., Camargo, S. J., & Galewsky, J. (2012). Variations in Tropical Cyclone Genesis Factors in Simulations of the Holocene Epoch, *Journal of Climate*, 25(23), 8196-8211.

Lee, H.-J.; Jin, E.-K., (2021).Seasonality and Dynamics of Atmospheric Teleconnection from the Tropical Indian Ocean and the Western Pacific to West Antarctica, *Atmosphere*, 12, 849. https://doi.org/10.3390/atmos12070849.

Lenaerts, J. T. M., Ligtenberg, S. R., Medley, B., Van De Berg, W. J., Konrad, H., Nicolas, J. P., et al. (2018). Climate and surface mass balance of coastal West Antarctica resolved by regional climate modelling. *Annals of Glaciology*, 59(76pt1), 29–41. https://doi.org/10.1017/aog.2017.42

Li, X., Gerber, E. P., Holland, D. M., & Yoo, C. (2015). A Rossby Wave Bridge from the Tropical Atlantic to West Antarctica, *Journal of Climate*, 28(6), 2256-2273. https://doi.org/10.1175/JCLI-D-14-00450.1

Lou, J., O'Kane, T.J. & Holbrook, N.J. (2021). Linking the atmospheric Pacific-South American mode with oceanic variability and predictability. *Commun Earth Environ* 2, 223 (2021). https://doi.org/10.1038/s43247-021-00295-4

Maclennan, M. L., & Lenaerts, J. T. (2021). Large-Scale Atmospheric Drivers of Snowfall Over Thwaites Glacier, Antarctica. *Geophysical Research Letters*, 48 (17), e2021GL093644. Retrieved from https://doi.org/10.1029/2021GL093644 doi: 10.1029/2021GL093644

Marshall, G. J., and Thompson, D. W. J. (2016), The signatures of large-scale patterns of atmospheric variability in Antarctic surface temperatures, *J. Geophys. Res. Atmos*., 121, 3276–3289, doi:10.1002/2015JD024665.

Marshall, G.J., Thompson, D.W. and van den Broeke, M.R., (2017). The signature of Southern Hemisphere atmospheric circulation patterns in Antarctic precipitation. *Geophysical Research Letters*, 44(22), pp.11-580.

Mattingly, K. S., T. L. Mote, and Xavier Fettweis. "Atmospheric river impacts on Greenland Ice Sheet surface mass balance." *Journal of Geophysical Research: Atmospheres* 123.16 (2018): 8538-8560.

Nuncio, M., & Yuan, X. (2015). The Influence of the Indian Ocean Dipole on Antarctic Sea Ice, *Journal of Climate*, 28(7), 2682-2690. Retrieved Mar 17, 2022, from https://journals.ametsoc.org/view/journals/clim/28/7/jcli-d-14-00390.1.xml

O'Brien, Travis Allen and Wehner, Michael F and Payne, Ashley E. and Shields, Christine A and Rutz, Jonathan J. and Leung, L. Ruby and Ralph, F. Martin and Marquardt Collow, Allison B. and Guan, Bin and Lora, Juan Manuel and et al., (2021). Increases in Future AR Count and Size: Overview of the ARTMIP Tier 2 CMIP5/6 Experiment. *Journal of Geophsyical Research-Atmospheres*, https://agupubs.onlinelibrary.wiley.com/doi/10.1029/2021JD036013

Phillips, A. S., C. Deser, and J. Fasullo, (2014). A New Tool for Evaluating Modes of Variability in Climate Models. *EOS*, 95, 453-455, doi: 10.1002/2014EO490002.

Pohl, B., Favier, V., Wille, J., Udy, D. G, Vance, T. R, Pergaud, J., et al. (2021). Relationship between weather regimes and atmospheric rivers in East Antarctica. *Journal of Geophysical Research: Atmospheres*, 126, e2021JD035294. https://doi.org/10.1029/2021JD035294

Power, S., Lengaigne, M., Capotondi, A., Khodri, M., Vialard, J., Jebri, B., Guilyardi, E., McGregor, S., Kug, J.S., Newman, M. and McPhaden, M.J., 2021. Decadal climate variability in the tropical Pacific: Characteristics, causes, predictability, and prospects. *Science*, *374*(6563), p.eaay9165.

Ralph, F. M., Dettinger, M. D., Cairns, M. M., Galarneau, T. J., & Eylander, J. (2018). Defining "Atmospheric River": How the Glossary of Meteorology Helped Resolve a Debate, *Bulletin of the American Meteorological Society*, 99(4), 837-839.

Raphael, M. N., Marshall, G. J., Turner, J., Fogt, R. L., Schneider, D., Dixon, D. A., Hosking, J. S., Jones, J. M., & Hobbs, W. R. (2016). The Amundsen Sea Low: Variability, Change, and Impact on Antarctic Climate, *Bulletin of the American Meteorological Society*, 97(1), 111-121. https://journals.ametsoc.org/view/journals/bams/97/1/bams-d-14-00018.1.xml

Rutz, J.J, Shields, C.A., Lora, J.M, Payne, A.E., Guan, B., Ullrich, P., O'Brien, T., Leung, L.-Y., Ralph, F.M., Wehner, M., Brands, S., Collow, A., Goldenson, N., Gorodetskaya, I., Griffith, H., Hagos, S., Kashinath, K., Kawzenuk, B., Krishnan, H., Kurlin, V., Lavers, D., Magnusdottir, G., Mahoney, K., McClenny, E., Muszynski, G., Nguyen, P.D., Prabhat, Qian, Y., Ramos, A.M., Sarangi, C., Sellars, S., Shulgina, T., Tome, R., Waliser, D., Walton, D., Wick, G., Wilson, A., Viale, M., (2019), The Atmospheric River Tracking Method Intercomparison Project (ARTMIP): Quantifying Uncertainties in Atmospheric River Climatology, *Journal of Geophysical Research-Atmospheres* , https://doi.org/10.1029/2019JD030936.

Shields, C.A., J.J. Rutz, L.R. Leung, F.M. Ralph, M. Wehner, T. O’Brien, and R. Pierce, (2019). Defining Uncertainties Through Comparison of Atmospheric River Tracking Methods. *Bull. Amer. Meteor. Soc*., 0, https://doi.org/10.1175/BAMS-D-18-0200.1 .

Shields, C. A., Rutz, J. J., Leung, L.-Y., Ralph, F. M., Wehner, M., Kawzenuk, B., Lora, J. M., McClenny, E., Osborne, T., Payne, A. E., Ullrich, P., Gershunov, A., Goldenson, N., Guan, B., Qian, Y., Ramos, A. M., Sarangi, C., Sellars, S., Gorodetskaya, I., Kashinath, K., Kurlin, V., Mahoney, K., Muszynski, G., Pierce, R., Subramanian, A. C., Tome, R., Waliser, D., Walton, D., Wick, G., Wilson, A., Lavers, D., Prabhat, Collow, A., Krishnan, H., Magnusdottir, G., and

Nguyen, P. (2018), Atmospheric River Tracking Method Intercomparison Project (ARTMIP): project goals and experimental design, *Geosci. Model Dev.*, 11, 2455-2474, https://doi.org/10.5194/gmd-11-2455-2018, 2018.

Spensberger, C., Reeder, M. J., Spengler, T., & Patterson, M. (2020). The Connection between the Southern Annular Mode and a Feature-Based Perspective on Southern Hemisphere Midlatitude Winter Variability. *Journal of Climate*, 33(1), 115–129. https://doi.org/10.1175/JCLI-D-19-0224.1

Terpstra, A., Gorodetskaya, I. V., & Sodemann, H. (2021). Linking sub-tropical evaporation and extreme precipitation over East Antarctica: An atmospheric river case study. *Journal of Geophysical Research: Atmospheres*, 126, e2020JD033617. https://doi.org/10.1029/2020JD033617

Turner, J., Phillips, T., Hosking, J. S., Marshall, G. J., & Orr, A. (2013). The Amundsen Sea low. *International Journal of Climatology*, 33(7), 1818–1829. https://doi.org/10.1002/joc.3558

Turner, J, Marshall, GJ, Clem, K, Colwell, S, Phillips, T, Lu, H. (2019). Antarctic temperature variability and change from station data. *Int J Climatol*, 40: 2986– 3007. https://doi.org/10.1002/joc.6378.

Turner, J. et al. (2019). The dominant role of extreme precipitation events in Antarctic snowfall variability. *Geophys. Res. Lett*. 46, 3502–3511.

Turner, J., Lu, H., King, J. C., Carpentier, S., Lazzara, M., Phillips, T., & Wille, J. (2022). An extreme high temperature event in coastal East Antarctica associated with an atmospheric river and record summer downslope winds. *Geophysical Research Letters*, 49, e2021GL097108. https://doi.org/10.1029/2021GL097108.

Wille, J.D., Favier, V., Dufour, A. et al. 2019). West Antarctic surface melt triggered by atmospheric rivers. *Nat. Geosci*. 12, 911–916. https://doi.org/10.1038/s41561-019-0460-1

Wille, J. D., Favier, V., Gorodetskaya, I. V., Agosta, C., Kittel, C., Beeman, J. C., et al. (2021). Antarctic atmospheric river climatology and precipitation impacts. *Journal of Geophysical Research: Atmospheres*, 126, e2020JD033788. https://doi.org/10.1029/2020JD033788.

Wille, J.D., Favier, V., Jourdain, N., et al. , (2022), The Atmospheric River Threat to Antarctic Peninsula Ice-Shelf Stability, 03 September 2021, PREPRINT (Version 1) available at Research Square [https://doi.org/10.21203/rs.3.rs-828007/v1]

Yan, Q., Wei, T., Korty, R.L., Kossin, J.P., Zhang, Z. and Wang, H., (2016). Enhanced intensity of global tropical cyclones during the mid-Pliocene warm period. *Proceedings of the National Academy of Sciences*, 113(46), pp.12963-12967.

Geophysical Research Letters

Supporting Information for

Evaluating Uncertainty and Modes of Variability for Antarctic Atmospheric Rivers

Christine A. Shields[1], Jonathan D. Wille[2], Allison B. Marquardt Collow[3,4], Michelle Maclennan[5], Irina V. Gorodetskaya[6]

[1]National Center for Atmospheric Research, Climate and Global Dynamics Laboratory, Boulder, Colorado

[2]Institut des Géosciences de l'Environnement, CNRS/UGA/IRD/G-INP, Saint Martin d'Hères, France

[3]University of Maryland Baltimore County, Baltimore, MD

[4]Global Modeling and Assimilation Office, NASA Goddard Space Flight Center, Greenbelt, MD

[5]University of Colorado, Department of Atmospheric and Oceanic Science, Boulder, Colorado

[6]CESAM – Centre for Environmental and Marine Studies, Department of Physics, University of Aveiro, Aveiro, Portugal

Corresponding author: Christine A. Shields (shields@ucar.edu)

Contents of this file

Introduction

Details for Antarctic-specific Wille ARDTs and computation of MOVs are provided as text. An Antarctic regional map, ARTMIP climatology frequency and seasonal cycle metrics for both Tier 1 and Tier 2 ARTMIP projects are provided as figures. ARTMIP ARDTs included in this study, with associated references and DOIs are provided in table format. Basic state figures for MOVs are provided for both spatial pattern and timeseries.

Text S1.

Standard IVT and IWV calculation

Traditional ARDTs designed for the mid-latitudes typically apply moisture thresholds using the quantity called integrated vapor transport (IVT), calculated as Eq. (1), which combines specific humidity with both zonal (u) and meridional (v) as such:

$$(1)\ \mathrm{IVT} = -\frac{1}{g}\int_{Pb}^{Pt} (q\ \boldsymbol{V}h)\ dp$$

where q is the specific humidity, $\mathbf{V}_h$ is the horizontal wind vector, Pb is pressure at the bottom of the atmosphere, typically 1000 hPa, Pt is at the top of the atmosphere, typically 200hPa, and g is the acceleration due to gravity.

Identification based solely on moisture stream, or integrated water vapor (IWV) (Eq. 2) is also commonly used and is expressed as Eq. (2):

$$(2)\ \mathrm{IWV} = -\frac{1}{g}\int_{Pb}^{Pt} q\ dp$$

which integrates the total column water without any wind information (Shields et al., 2018).

Antarctic AR Detection Tool, Wille_vIVT and Wille_IWV

Moisture thresholds for the Wille “vIVT” ARDT, use anomalies of the *meridional* component to the integrated water vapor (vIVT) expressed as

$$\text{vIVT} = -\frac{1}{g}\int_{surface}^{top} (q\ v h)\ dp$$

where v_h is the meridional component of the wind, q is the specific humidity, p atmospheric pressure (hPa). and g is the acceleration due to gravity. Full reanalysis levels are used.

The Wille "IWV" ARDT algorithm uses integrated water vapor anomalies similar to the traditional method with the exception of using full reanalysis model levels. It can be expressed as

$$\text{IWV} = -\frac{1}{g}\int_{surface}^{top} q\ dp$$

where q is the specific humidity, p atmospheric pressure (hPa), and g is the acceleration due to gravity.

Both Wille_vIVT and Wille_IWV compute moisture thresholds defined as the 98th percentile in mean monthly climatological IWV or vIVT for all grid cells calculated using reanalysis data. Geometry requirements focus on the latitudinal footprint. Shapes are tested for a minimum continuous 20^o latitude span between 37.5^o S - 80.0^o S. More details and application can be found in Wille et al. 2019 and Wille et al. 2021.

ARTMIP ARDTs

A summary of all over ARDTs is found in Table S1.

Text S2.

Decadal Modes of Variability

Decadal modes include both the Southern Annular Mode (SAM) and the Pacific Decadal Oscillation (PDO). SAM is calculated classically as the leading EOF of the detrended 500 hPa geopotential anomalies for the southern hemisphere from 20^oS to 90^oS. Principle component (PC) time series are regressed onto precipitation and 850 hPa temperature for AR days to show correlation of AR characteristics with SAM. PDO is defined as the leading principal component of the North Pacific Ocean (20:70°N, 110°E:100°W) of the detrended sea surface temperature anomalies. Spatial patterns and PC timeseries for both SAM and PDO are shown in Supplemental Figure S2.

Interannual Modes of Variability

Interannual modes include the 2nd Pacific South American pattern, (PSA2), and the Indian Ocean Dipole (IOD), both in and out of phase with El Niño Southern Oscillation (ENSO). The first pattern of PSA (PSA1) is not shown because it lacks significance with AR days. PSA2 is defined as the 3rd EOF of detrended 500 hPa geopotential height anomalies, which is the same domain and approach as SAM. Not only does EOF3 of 500 hPa geopotential height have implications for Antarctic ARs, it has also been shown as important for extratropical moisture transport, especially for western North America (J.P. O'Brien personal communication). The

IOD is calculated by differencing detrended, area-averaged sea surface temperature anomalies between 10°S-10°N and 50-70°E versus 0-10°S and 90-110°E. For ENSO, we choose to apply the combined Niño3.4 region to emphasize more centralized equatorial sea surface temperatures. Area-averaged SST anomalies for Niño3.4 are computed over 5°S-5°N and 120-170°W. For MOV analysis, the IOD index, both in and out of phase with ENSO, is regressed onto precipitation and 850 hPa temperatures for AR days. PSA2 and IOD patterns and timeseries are shown in Supplemental Figure S2.

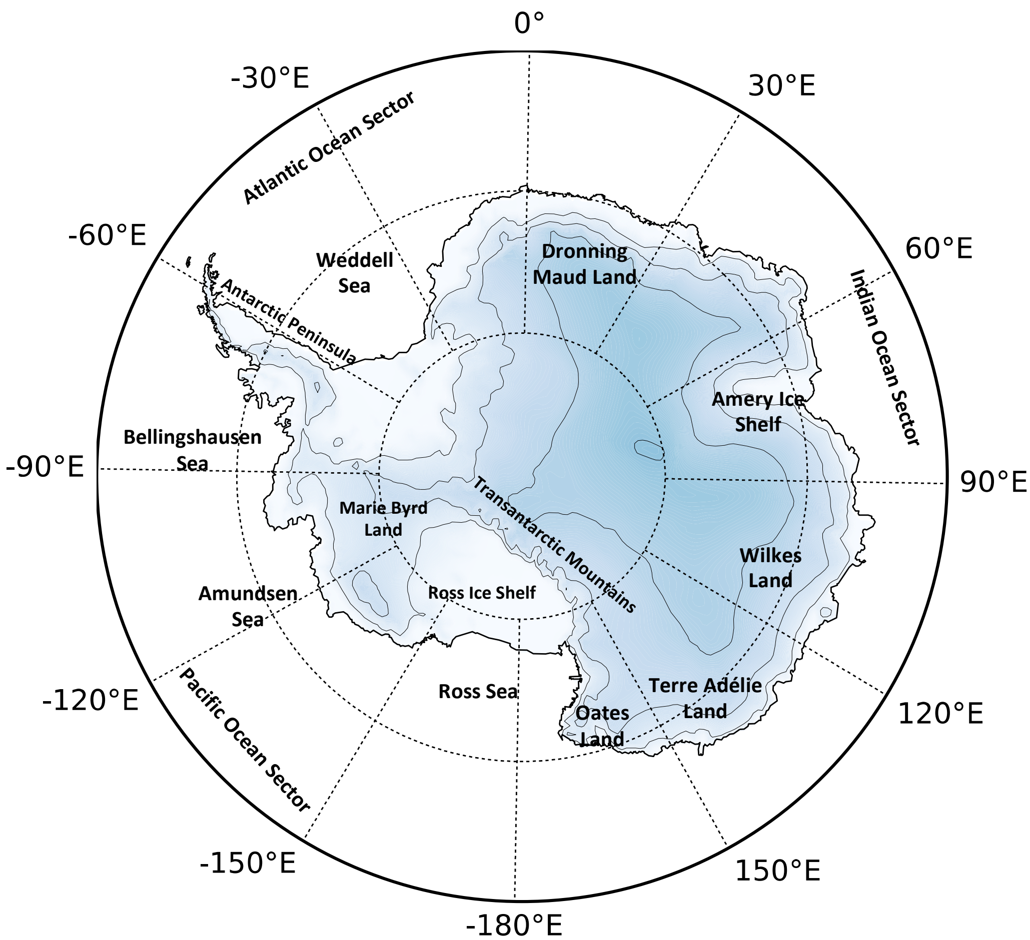

Figure S1. Antarctic map with labels identifying regions discussed in the main article. Blue shading and contours represent topography.

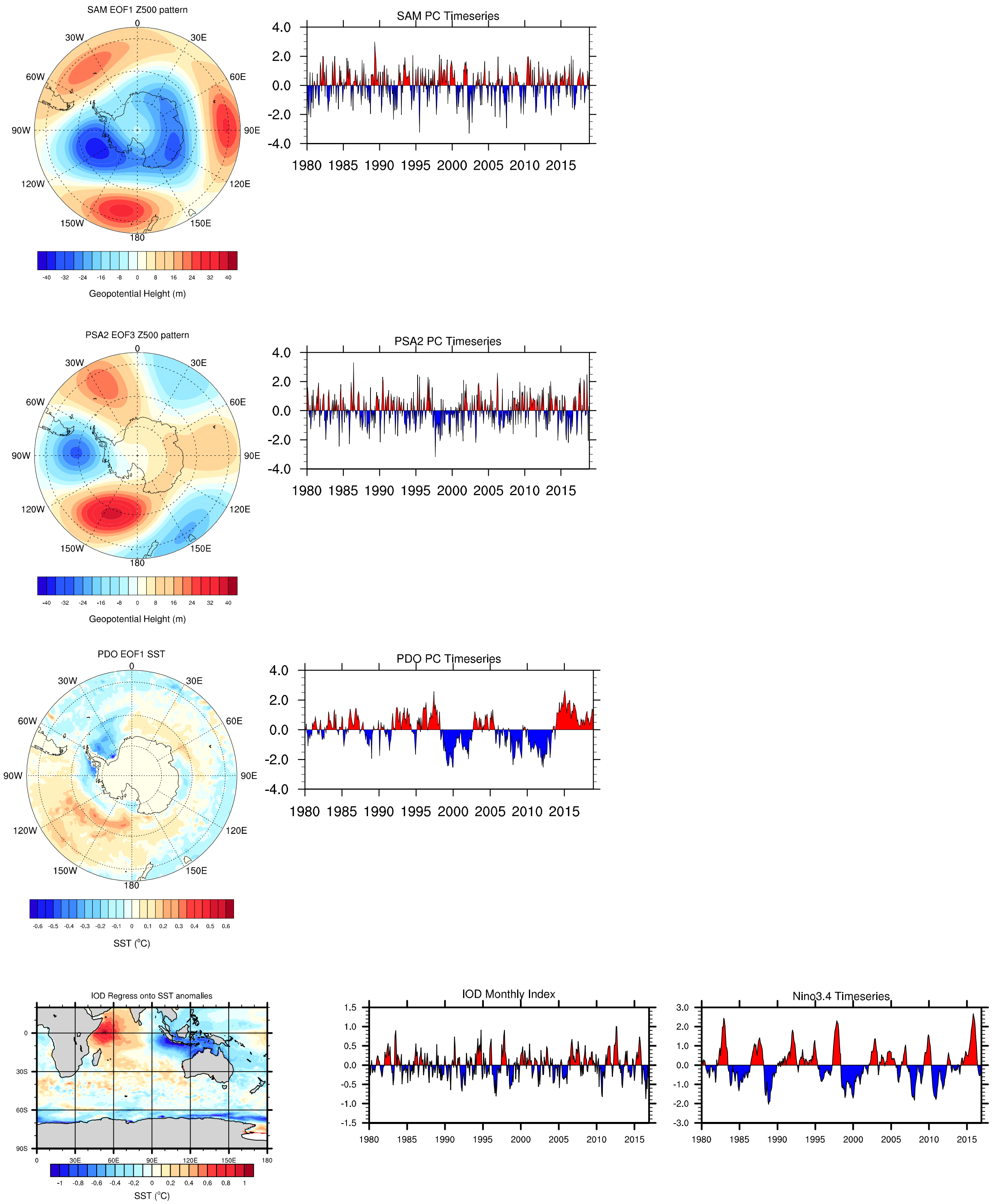

Figure S2. Modes of variability spatial patterns and timeseries for SAM (first row), PSA2 (second row), PDO (third row), IOD (fourth row). Nino3.4 timeseries is shown with IOD for reference.

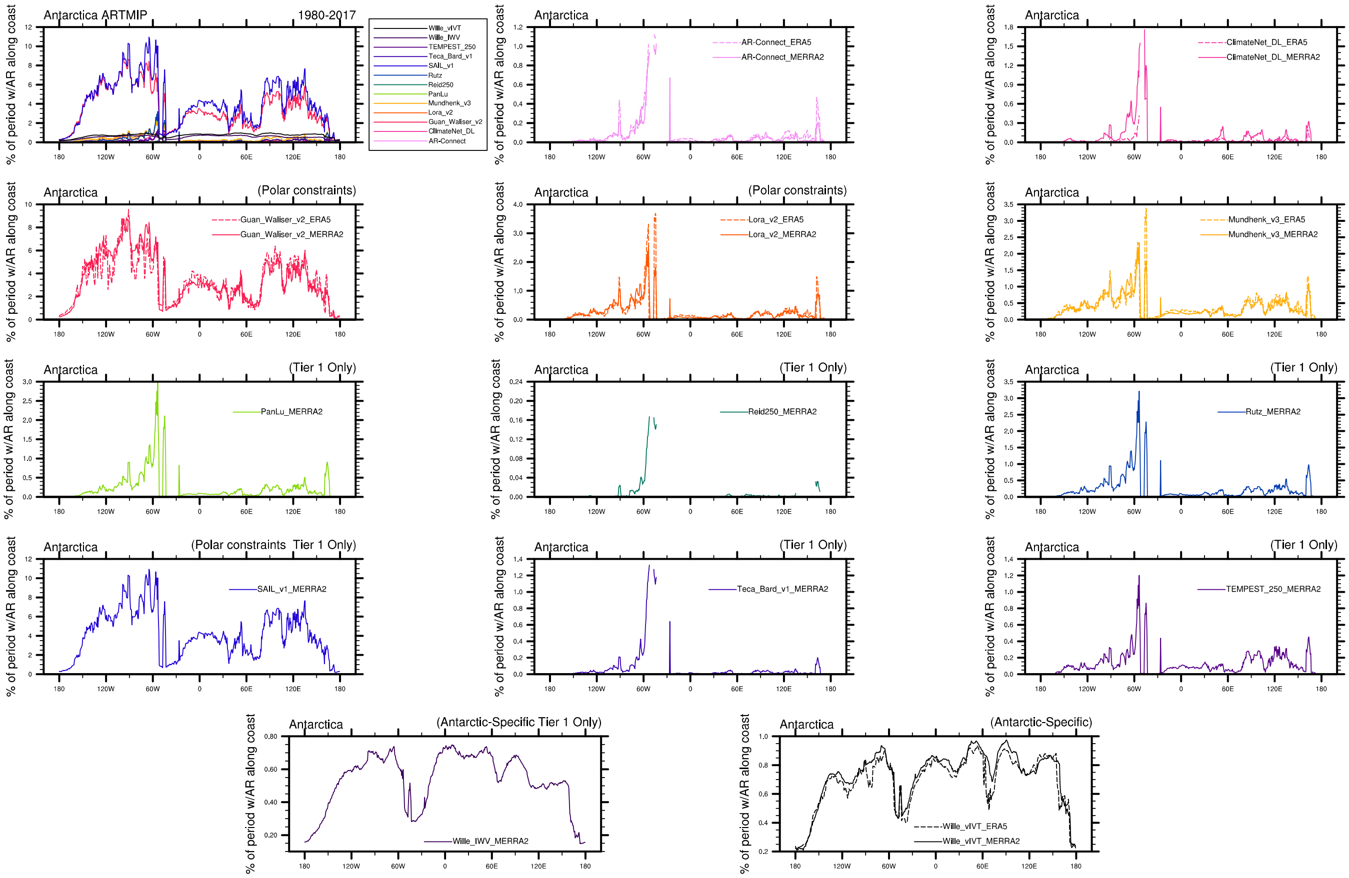

Figure S3. AR frequency ARTMIP Tier 1 and Tier 2 ARDTs (% time relative to analysis period across longitudinal transect around the continent of Antarctica for all methods Tier 1 (MERRA2 1980-2016) (upper left), and individually, Tier 1 and participating Tier 2 (all other panels) where ERA5 analysis base period is 2000-2019. Wille_vIVT and TEMPEST, Reid500, Mundhenk, and Guan_Waliser submitted extended-ERA5 periods, 1980-2019. ARDTs with polar constraints (P-ARTMIP) are noted in individual panel titles. Wille ARDTs capture ARs consistently across all longitudes where most other ARDTs preferentially detect the Antarctic Peninsula.

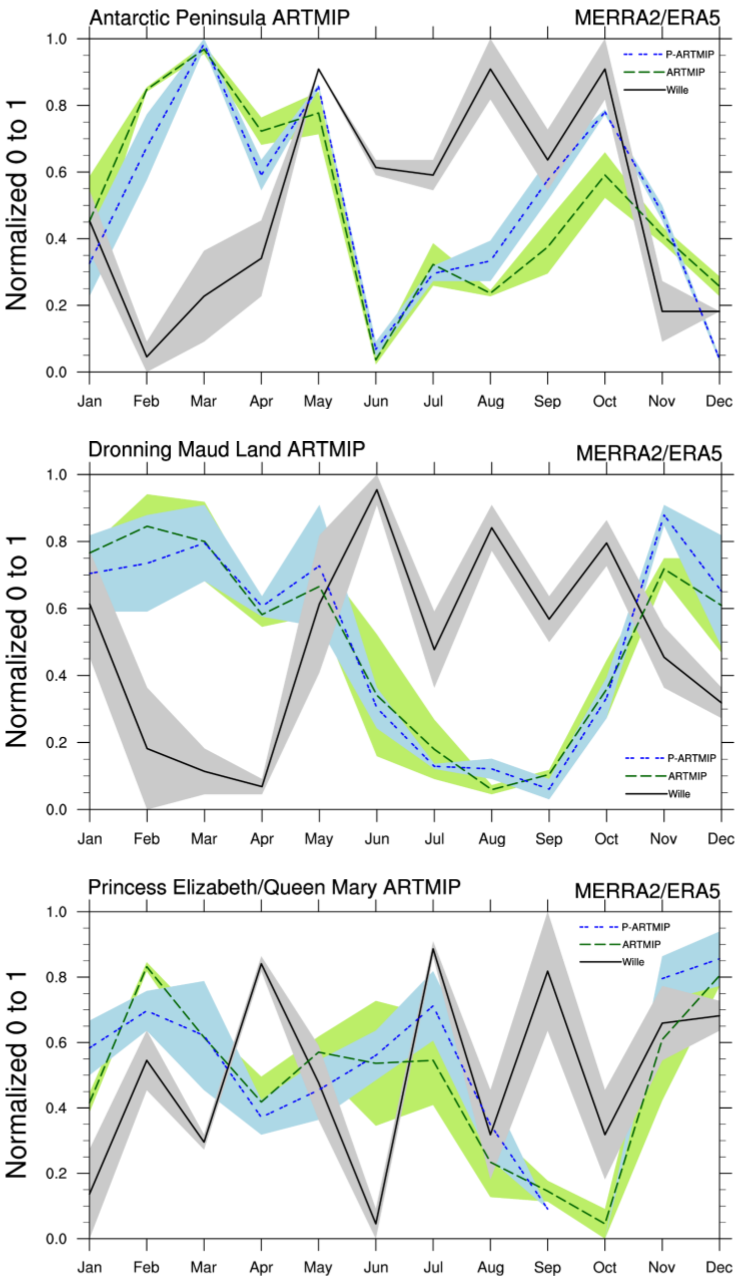

Figure S4. Same as Figure 2 in main text, except for regional locations around Antarctica, Antarctic Peninsula (a), East Antarctica, Dronning Maud Land (b), and East Antarctica, Princess Elizabeth and Queen Mary Land (c).

ARDT Name/Developer	**Type**	**Algorithm Summary**	**DOI Reference**
AR-Connect**	Global	Object identification; Absolute: IVT thresholds used = 700 kg/m/s for seeding, 300, for region growing; Time stitching, minimum 24-hour period; Global weighted centroid of AR event must be outside tropics (23.25 N - 23.25 S)	10.1029/2020JD033425
ClimateNet_DL**	Global	Deep learning based segmentation; Trained on ~500 expert labeled images; Threshold free; input fields are IWV, U850, V850, SLP; Time slice condition	10.5194/gmd-14-107-2021
Guan_Waliser_v2**	Global - Polar constraints	Length >2000km and length width ratio >2; Coherent IVT direction within 45° of AR shape orientation and with a poleward component; Relative: 85th percentile IVT; Absolute min requirement designed for polar locations: 100kg/m/s IVT; Time slice condition	10.1002/2015JD024257 10.1175/JHM-D-17-0114.1
Lora_v2**	Global - Polar constraints	Length >= 2000km; Relative/Absolute : IVT 225 kg/m/s above time/latitude dependent threshold using 30-day running mean and zonal average of IWV; Time slice condition	10.1016/j.epsl.2020.116293
Mundhenk_v3**	Global	>1400km length, aspect ratio 1:4, lat limit >16N/S, axis orientation based on IVT; Relative IVT percentiles and/or anomalies both temporal and spatial; Time slice condition	10.1175/JCLI-D-15-0655.1
PanLu	Global	1) Length>2000km; 2) Length-Width ratio>2; 3) sum of turning angle<360; 4) percentage within tropics < 95%; 5) 50% < percentage within tropics < 95% or percentage with IVT direction smaller than 15 degrees <50%; Two relative thresholds. Local threshold: smoothed 85% quantile IVT field using the Gaussian kernel density smoothing technique; regional threshold: the 80% quantile of IVT for all grids within 80N and 80S; Time stitching: last for at least 18 hours	10.1029/2018WR024407 10.1029/2020GL089477
Reid250	Global	Length > 2000km; Length-Width ratio > 2; orientation angle >10°; Absolute. IVT > 250 kg/m/s; IVT > 500 kg/m/s; Time slice condition	10.1029/2020JD032897
Rutz	Global	Length >= 2000km; Absolute: IVT (surface to 100mb) = 250kg/m/s; Time slice	10.1175/MWR-D-13-00168.1

		condition; low value on tropics	
SAIL_v1	Global - Polar constraints	Length >= 250km; Length-to-width >=5; Length is estimated along the "ridge" taking IVT into account; Width is the median of widths estimated in each point of AR ridge; Relative: IVT-IVT_RM >_ 100 kg/m/s. IVT_RM is climatological IVT running mean with 20-day windows; Time slice condition	Experimental
Teca_Bard_v1	Global	Runs 1,024 AR detectors simultaneously. Percentile threshold, minimum area, and filter latitude width are all sampled from a posterior distribution that is designed to optimize global AR counts relative to a dataset of AR counts from a set of experts.; Relative threshold (based on spatial percentile for each timestep); An inverted Gaussian filter is applied at the equator to damp out the ITCZ; Time slice condition	10.5194/gmd-13-6131-2020
TEMPEST (IVT threshold 250)	Global	Contains both an absolute threshold (typically set at IVT>250 kg/m/s) and a relative threshold (which uses a local Laplacian of IVT, typically set at del^2 IVT < -50k); Laplacian IVT thresholds most effective for widths >1000km; cluster size minimum = 120000km2; Time stitching condition, Global, but latitude >=15°	10.5194/gmd-10-1069-2017
Wille_IWV	Antarctic Specific	Length > 20° (2000 km) equatorward with no breaks; Defined as AR landfall if AR shape overlaps a land grid cell; Relative > 98th percentile IWV based on monthly climatological means; Time slice condition	10.1038/s41561-019-0460-1 10.1029/2020JD033788
Wille_vIVT**	Antarctic Specific	Length > 20° (2000 km) equatorward with no breaks; Defined as AR landfall if AR shape overlaps a land grid cell; Relative > 98th percentile vIVT based on monthly climatological means; Time slice condition	10.1038/s41561-019-0460-1 10.1029/2020JD033788

Supplemental Table S1. ARTMIP ARDTs and references are listed. 13 Tier 1 (MERRA2) and 6 Tier 2 (ERA5) ARDTS are included in this study. Selection was determined by including any catalogue that captured ARs over Antarctica. Regression and MOV analysis was only performed on ARDTs with polar constraints (5 ARDTs) to minimize error by only applying ARDTs fit for purpose. **ARDTs have both Tier 1 (MERRA2) and Tier 2 (ERA5) catalogue entries. Algorithm summaries are also available on the ARTMIP webpage (https://www.cgd.ucar.edu/projects/artmip/algorithms.html)

References for Supplemental

Guan, B., and D. E. Waliser, (2015). Detection of atmospheric rivers: evaluation and application of an algorithm for global studies. J. Geophys. Res. Atmos., 120, 12, 514–535.

Kashinath, K., Mudigonda, M., Kim, S., Kapp-Schwoerer, L., Graubner, A., Karaismailoglu, E., Von Kleist, L., Kurth, T., Greiner, A., Mahesh, A. and Yang, K., (2021). ClimateNet: an expert-labeled open dataset and deep learning architecture for enabling high-precision analyses of extreme weather. Geoscientific Model Development, 14(1), pp.107-124.

Mundhenk, B. D., E. A. Barnes, and E. D. Maloney (2016). All-season climatology and variability of atmospheric river frequencies over the North Pacific, J. Climate, 29, 4885 4903.

O'Brien, T. A., Risser, M. D., Loring, B., Elbashandy, A. A., Krishnan, H., Johnson, J., Patricola, C. M., O'Brien, J. P., Mahesh, A., Arriaga Ramirez, S., Rhoades, A. M., Charn, A., Inda Díaz, H., & Collins, W. D. (2020). Detection of atmospheric rivers with inline uncertainty quantification: TECA-BARD v1.0.1. Geoscientific Model Development, 13(12), 6131–6148.

Pan, M. and Lu, M. (2019). A Novel Atmospheric River Identification Algorithm, Water Resources Research, 2019, 55: 6069-6087.

Reid, K. J., King, A. D., Lane, T. P., & Short, E. (2020). The sensitivity of atmospheric river identification to integrated water vapor transport threshold, resolution, and regridding method. Journal of Geophysical Research: Atmospheres, 125, e2020JD032897.

Rutz, J. J., W. J. Steenburgh, and F. M. Ralph, (2014). Climatological characteristics of atmospheric rivers and their inland penetration over the western United States. Mon. Wea. Rev., 142, 905–920.

Shearer, E. J., Nguyen, P., Sellars, S. L., Analui, B., Kawzenuk, B., Hsu, K., et al. (2020). Examination of global midlatitude atmospheric river lifecycles using an object-oriented methodology. Journal of Geophysical Research: Atmospheres, 125, e2020JD033425.

Shields, C. A., Rutz, J. J., Leung, L.-Y., Ralph, F. M., Wehner, M., Kawzenuk, B., Lora, J. M., McClenny, E., Osborne, T., Payne, A. E., Ullrich, P., Gershunov, A., Goldenson, N., Guan, B., Qian, Y., Ramos, A. M., Sarangi, C., Sellars, S., Gorodetskaya, I., Kashinath, K., Kurlin, V., Mahoney, K., Muszynski, G., Pierce, R., Subramanian, A. C., Tome, R., Waliser, D., Walton, D., Wick, G., Wilson, A., Lavers, D., Prabhat, Collow, A., Krishnan, H., Magnusdottir, G., and Nguyen, P. (2018). Atmospheric River Tracking Method Intercomparison Project (ARTMIP): project goals and experimental design, *Geosci. Model Dev.*, 11, 2455-2474, https://doi.org/10.5194/gmd-11-2455-2018, 2018.

Skinner, C.B., Lora. J.M. Payne, A. E., Pouslen, C. J., (2020), Atmospheric river changes shaped mid-latitude hydroclimate since the mid-Holocene, Earth and Planetary Science Letters, 541.

Ullrich, P.A. and Zarzycki, C.M., (2017). TempestExtremes: A framework for scale-insensitive pointwise feature tracking on unstructured grids. Geoscientific Model Development, 10(3), pp.1069-1090.

Wille, J.D., Favier, V., Dufour, A. et al. (2019). West Antarctic surface melt triggered by atmospheric rivers. *Nat. Geosci*. 12, 911–916. https://doi.org/10.1038/s41561-019-0460-1

Wille, J. D., Favier, V., Gorodetskaya, I. V., Agosta, C., Kittel, C., Beeman, J. C., et al. (2021). Antarctic atmospheric river climatology and precipitation impacts. Journal of Geophysical Research: Atmospheres, 126, e2020JD033788.